FISEVIER

Contents lists available at ScienceDirect

Journal of Wind Engineering & Industrial Aerodynamics

journal homepage: www.elsevier.com/locate/jweia



Numerical analysis of the mirco-particles distribution inside an underground subway system due to train piston effect



Tahereh Izadi ^{a,b}, Mozaffar Ali Mehrabian ^a, Goodarz Ahmadi ^c, Omid Abouali ^{b,*}

- ^a Department of Mechanical Engineering, Shahid Bahonar University of Kerman, Iran
- ^b School of Mechanical Engineering, Shiraz University, Iran
- ^c Department of Aeronautical and Mechanical Engineering, Clarkson University, Potsdam, NY, USA

ARTICLE INFO

Keywords: Numerical modeling Particle distribution Piston effect Dynamic mesh Subway system Train brake

ABSTRACT

The train movement in a model of the subway tunnels and stations with a side-platform was simulated using a 3D computational model. The impact of airflow mainly due to piston effect on distribution of particles generated due to the train braking was investigated. The unsteady RANS and energy equations were solved using the dynamic mesh technique with an Eulerian approach. The particle trajectories were evaluated by the Lagrangian approach. The particle concentration in different points of the station emitted due to the train braking is obtained and discussed. The results showed that when the train enters the station while braking, a fraction of particles is transported and spread into the platform areas. Some of the generated particles, however, were accumulated in the rear of the train. When the train stops, these particles entered into the station due to continuation of the piston effect. The simulations showed that particles would spread in the platform and penetrate into the staircases and ticket hall, and even disperse into the outside ambient. The results also demonstrated that some of the particles released from the braking system of the train could penetrate into the train through the ventilation system of the passenger cars.

1. Introduction

Considering the wide use of subway as a convenient public transport system, many people spend considerable amounts of time inside the subway stations. Subway systems are known as one of the efficient and environmentally friendly transit systems. Despite their benefits, many subway systems have problems in terms of underground air quality. Previous studies in subway systems of various cities around the world showed that particulate matter (PM) concentrations are usually higher in these environments than PM measurements in the ambient air. This is because of generation and accumulation of PM in a closed environment of subway system (Nieuwenhuijsen et al. (2007)). It is reported that PM10 and PM2.5 concentrations in subway stations of Paris were about 5–30 times higher than outdoor (Raut et al. (2009)), while they are about 0.65-1.75 times higher than outdoor in Taipei subway stations (Cheng et al. (2008)). The concentrations in subway stations of Buenos Aires were reported to be 3 times higher than outdoor (Murruni et al. (2009)). In addition, as shown by Karlsson et al. (2005), the subway particles in comparison to nearby busy urban street were eight times more genotoxic and four times more probable to bring about oxidative stress in the lung cells. Researchers have reported PM levels in different subway systems in numerous cities worldwide (Berlin (Fromme et al. (1998)), Boston (Levy et al. (2000)), Tokyo (Furuya et al. (2001)), London (Seaton et al. (2005)), Guangzhou (Chan et al. (2002)), Stockholm (Johansson and Johansson (2003)), New York (Chillrud et al. (2004)), Mexico City (Mugica-Álvarez et al. (2012)), Helsinki (Aarnio et al. (2005)), Rome (Ripanucci et al. (2006)), Prague (Braniš (2006)), Beijing (Cui et al. (2016)), Seoul (Kim et al. (2008); Li et al. (2019a)), Buenos Aires (Murruni et al. (2009)), Sydney (Knibbs and de Dear (2010)), Shanghai (Ye et al. (2010)), Los Angeles (Kam et al. (2011)), Barcelona (Moreno et al. (2017)), Milan (Colombi et al. (2013)) and Nanjing (Shen and Gao (2019))). The data obtained in various underground subway systems are different because there are several parameters influencing the PM concentration results, such as ventilation and air conditioning systems, design of subway system, the materials of train wheel and rail-track, braking mechanisms, system age, train frequency and passengers density (Martins et al. (2015b); Moreno et al. (2014)).

Martins et al. (2015a) measured the average PM_{2.5} concentrations at several subway stations as well as outdoor environment. Their findings showed the lower concentrations in outdoor in comparison to the subway

E-mail address: abouali@shirazu.ac.ir (O. Abouali).

 $^{^{\}ast}$ Corresponding author.

stations. Therefore, it can be concluded that the air quality in the subway stations is not affected significantly by outdoor $PM_{2.5}$ concentrations and the motion of the trains and the passengers' movement in the subway system are the main source of $PM_{2.5}$ particles in the underground stations. The same results were presented by some of the above studies.

To investigate indoor sources of subway particles, an experiment is conducted by Jung et al. (2010). Subway particle samples were collected at four underground subway stations in Seoul. The samples were collected in tunnels, near ticket offices, outdoors and at platforms. They found that the samples collected in tunnels and platforms contain mainly Fe-containing particles with relative abundances of 75-91%. They also found that as the distance of sampling locations from the tunnel and railway increases, the amounts of Fe-containing particles decreases. Therefore, the Fe-containing particles were originating from tunnels and railway. In addition, Fe and Si, with some amounts of Mn, Cr, Cu, Ca, and K are reported to be the main chemical constituent of underground subway PM according to different studies (Sitzmann et al. (1999); Birenzvige et al. (2003); Chillrud et al. (2004); Aarnio et al. (2005); Seaton et al. (2005); Nieuwenhuijsen et al. (2007); Salma et al. (2009); Murruni et al. (2009)). Thus, it can be concluded that, the main source of subway aerosol particles are abrasion of rail tracks and wheels, catenary and brake pads (Querol et al. (2012)).

Brake pads on wheel-mounted disc brakes are often used in rail transport. When the train brakes, the wearing process of the disc and the pads produces particles. These particles may become airborne and harmful to human health (Abbasi et al. (2011)). Prior studies show that these airborne wear particles concentrations in urban areas may exceed the levels presented in EU guideline 96/62/EG (Olofsson et al. (2009)). Understanding the wear mechanisms may provide a tool to control the distribution of wear particles in subway systems. Notably, only a few studies have examined the characteristics of particles generated from railway components. In these studies, a pin-on-disc set-up was used to study the airborne particles generated from various materials under various test conditions. Abbasi et al. (2011) and Abbasi et al. (2012b) study the airborne wear particles from typical organic brake pads against steel brake disc. The study was conducted through a series of full-scale field and laboratory tests using a pin-on-disc machine. For their field tests, they considered two airborne particle sampling points, one near a pad-rotor disc brake contact and a second in the middle of the axle. They showed that iron and then copper were the main elements in the two sampling points, and the wear rate and particle generation increase with increasing braking force. They also found that the number of generated particles is higher when the applied load increases, but the particle size distribution was not dependent on the applied load. Three particle size regimes were captured as follows: a peak of around 100 nm, 0.35 μm and 3-6 µm in diameter for the ultra-fine, fine and coarse regions, respectively. These peaks are also obtained in other studies with different contact conditions (Olofsson et al. (2009); Sundh et al. (2009); Wahlström et al. (2009)). The measurements of Fridell et al. (2010) on the abrasion particles produced by three types of train showed the particles size with a maximum around 1 µm for all the train types. In a related work, Fridell et al. (2011) proved that there must be a correlation between braking and particle emissions. Based on their study very high particle emissions seemed to be produced by mechanical braking. In accordance to other studies, they also showed that iron is the dominating element.

Overall, many subway stations all over the world are reported to have high PM concentrations, with significant portion of iron-containing particles. These particles were mostly generated due to wearing process of the brake pad and their sizes were measured in various experimental researches. However, there are not many numerical studies on the simulation of distribution of particulates in underground subway stations. In addition, very few studies have investigated the particle distribution from a moving source such as train. Thus, in this study, the train movement along stations and connecting tunnels was simulated using the dynamic mesh technique. For increasing the reliability of the numerical

model, four stations were considered in the model including passenger platforms, stair cases, ticket halls and ventilation system. The tunnels were double track and the stations were sided platform type. The particle generation due to the braking was simulated. Particles characteristics (size distribution and density) were estimated using the information available in the literature. The train-induced airflow field and the associated particle trajectories were analyzed. In addition, the number of particles entering the train model through the air conditioning system was also investigated. The present work provided the 3D simulations for the dispersion and spread of brake generated particulates in the subway station due to train movement.

2. Model description

2.1. 3D computational model and dynamic mesh technique

In this study, the train model is assumed to be made of a series of blocks for simulation purposes. The computational domain for the tunnel and stations that resembles a typical subway line is shown in Fig. 1a. This figure shows that four stations are included in the model in order to ensure the accuracy of the predictions for the main tunnel. Each station has a ticket hall connected to the outside ambient air by two main doors. The ticket hall is also connected to the platform by two sets of staircases on both sides. Therefore, as seen from Fig. 1b, there are four way-outs in each platform station, two on the right and the other two on the left. Each platform has sixty air grilles (each 0.425 m \times 0.825 m with an air exchange rate of 1200 cfm) on the roof as shown in Fig. 1b. All tunnels are double track with one exhaust fan opening (3 m \times 6.68 m) connected to a middle shaft in the middle of each tunnel and two blower fan openings at the beginning and end of each tunnel. The middle exhaust fans exhausts 250,000 m³/h of air to the outside and each blower fan blows 80,000 m³/ h of air with the slope of 45° towards the tunnel center (Fig. 1a). The ticket hall, staircases and platform geometry are selected in a way to be consistent with those in Metro line 1-Phase 1 in Shiraz subway system. The important specifications of the model are shown in Fig. 1c and are listed in Table 1. It should be emphasized that since the particle release due to train braking is considered in this study, most of the discussions are focused on Station 3.

At the initial time, the train is placed in one of the stations (Station 2) on the left track. To separate the moving grids from stationary ones, four grid interfaces were used which surrounded the train (Fig. 1c). The moving grids are inside the interfaces and the stationary grids are outside them. The dynamic mesh technique of ANSYS-FLUENT software package was used to simulate the train movement and regenerate the computational mesh at each time step.

It should be pointed out that because of using the dynamic mesh technique and a huge computational domain, this 3D unsteady work becomes a heavy computational task and some simplifications have been performed. Since the station geometry might have a major impact on the piston effect variation and particle distribution inside subway system, a realistic model for the station was developed. A simple model of the train shape was assumed, however, more precise treatment for train shape, specially for the bogie and skirt model, is highly recommended for future work.

A structured computational grid is generated around the train which moves with that in the tunnels and stations (Fig. 2a). Finer grids are used near the train walls, fan openings and mostly for the destination station (Station 3). The height of the first cells near the walls, y, should be selected in a way that the non-dimensional y^+ value is maintained in an appropriate range which is $30 < y^+ < 300$, where $y^+ = \frac{\rho u_s y}{\mu}$. In this study, except for some points on the head of the train which the y + exceed to 750, the y^+ value was maintained in the preferred region. To show that the solutions are independent of the grids, the grid sensitivity analysis is performed. For this aim, a computational model with finer mesh sizes is generated. In this model,

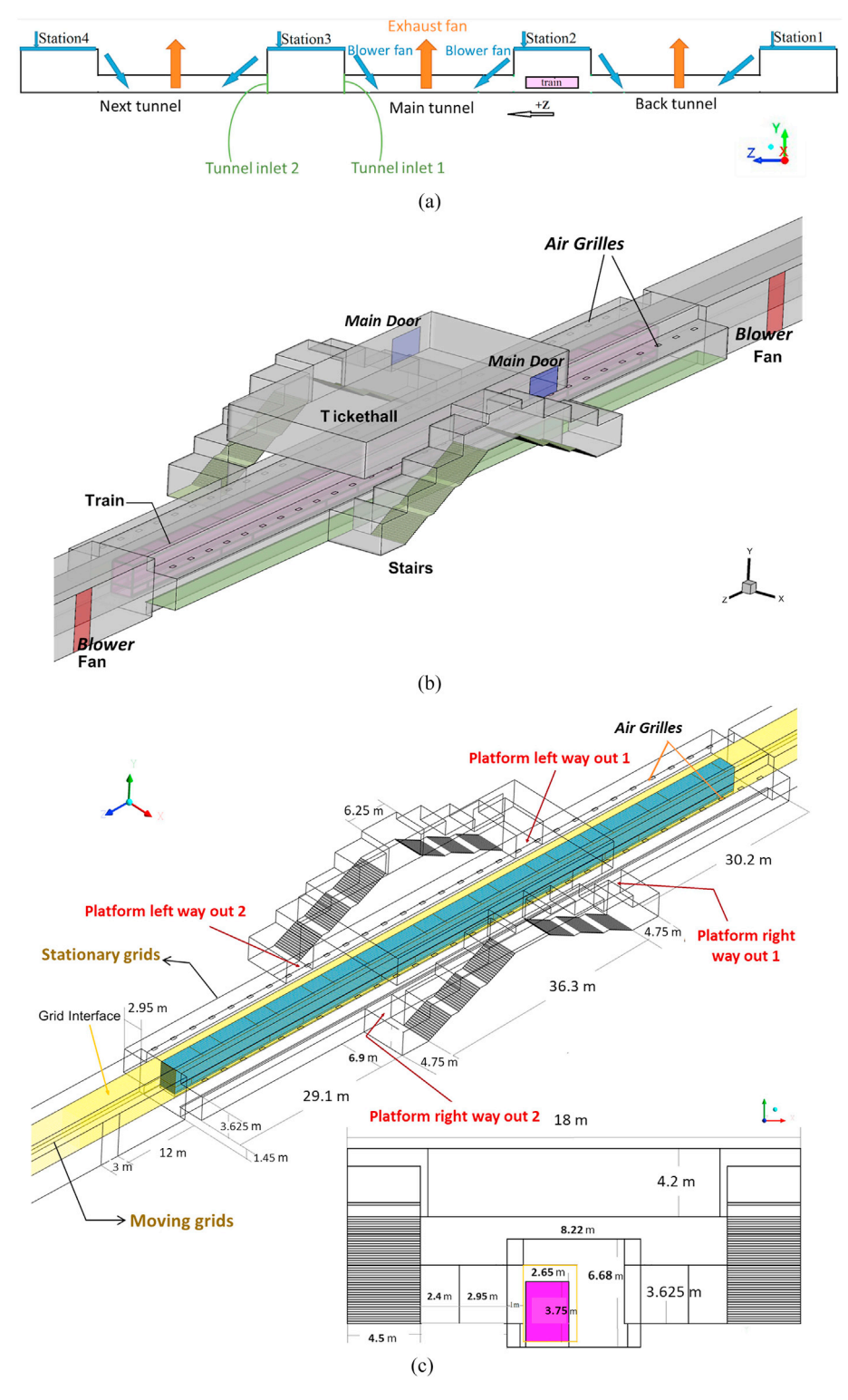


Fig. 1. (a). Computational domain for the tunnel and stations. (b) Schematic diagram of train and tunnel models with the train at the start position. (c) Schematic diagram of grid interface along the tunnel and computational domain cross sectional shape.

Tunnel and station specifications.

	Length	Width	Height
Train	100 m	2.65 m	3.7 m
Tunnel	1000 m	8.22 m	6.68 m
Platform	105 m	14 m	3.6 m
Ticket hall	39 m	18 m	4.2 m

the mesh sizes are reduced to 1/3 of that in the medium mesh sizes model for some parts of the model especially in the station 3 around the train walls. Fig. 2b compares the time variation of air mass flow rates from the Station 3 to the next tunnel (Tunnel inlet 2) for both meshes. This figure shows that the results of both meshes are approximately the same. Fig. 2c illustrates the time variation of average particle concentration on a surface located in the left side of the platform, 1 m above its floor. As can be seen from this figure, the

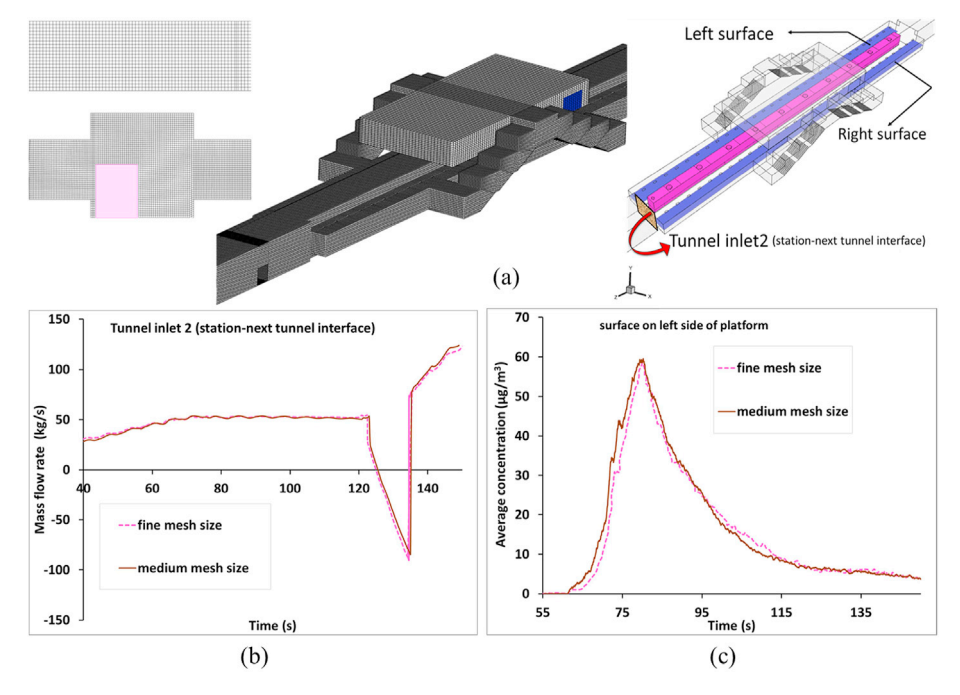


Fig. 2. (a) Schematic of computational meshes with the details of the 2D mesh around the train domain. (b) Comparison between different meshes for the air mass flow rates from the station to the next tunnel (Tunnel inlet 2) (c) Comparison between different meshes for the average particle concentration on a plane located 1 m above the left platform floor.

results of particle concentration for the medium mesh sizes are in good agreement with those for the fine mesh sizes. Therefore, the medium mesh sizes model with around 11 million cells is selected for this study. It is good to mention that the mesh sizes are selected based on the computational limitations, since the complexity of the geometrical model and particle numbers require a high computational cost. Using the computer system with 16 cores (Core (TM) i7-6900 k CPU @ 3.20 GHz) and memory of 40.0 GB, it takes around three weeks to simulate the train movement and particle distributions. Besides, the planar pressure waves are generated and propagated inside subway system due to the piston effect. These pressure waves are dominant inside subway system and the flow field can be approximated even as an axisymmetric (Izadi et al. (2019)). So the flow field is less sensitive to the grid sizes.

3. Numerical method

The unsteady forms of continuity and Reynolds Averaged Navier-Stokes (RANS) equations are used for simulating the compressible turbulent flow induced by the train movement. The RANS equations has been mainly applied for studying the piston effect inside a tunnel (Jiang et al. (2019); Li et al. (2019b); Zarnaghsh et al. (2019); Yang et al. (2018)). To include the effect of turbulence stresses, the k- ϵ model with standard wall-function approach for near-wall velocity was used. The constant of the law of the wall has been modified based on the roughness of the wall surfaces especially for the tunnels. Xue et al. (2014) studied the three-dimensional train-induced airflow in a subway station and tunnel numerically and experimentally. They showed that standard k– ϵ and RNG $k-\epsilon$ models are proper for turbulence models. Consequently, the same as the earlier works of Niu et al. (2018), Zhang et al. (2017), González et al. (2014) and Kim and Kim (2009), the k- ϵ model is applied in the present study so as to investigate the train-induced airflows. Having said that, the k-ω model is also examined in this study and the results proved to be very close to that of the k-ε model so they are not presented here for brevity. The details of the governing equations are available in the book by Wilcox (2006). It is good to mention that there is various installed equipment in the tunnel such as the cable tray, pipes for

fire-fighting waters, rail, electrical system and so on. This equipment mainly affects the friction drag in the tunnel. It is proposed by subway environmental design handbook (Kennedy (1976)) to use an equivalent roughness, between 1 and 2 cm, for the estimation of the friction factor of the tunnel wall. Therefore, in the present study, the mentioned equipment was not simulated and a roughness of 2 cm was used for the tunnel walls, instead. The air at the main doors, the first plane of Station 1, and the last plane of Station 4 are at atmospheric pressure. For the numerical calculations, the finite volume method along with the SIMPLE algorithm were used.

3.1. Discrete phase particle model

3.1.1. Equations for particle motion

The Lagrangian method is used to calculate the particle trajectory by solving the Newton's second law:

$$\frac{d\overrightarrow{\mathbf{u}}_{p}}{dt} = F_{D}(\overrightarrow{\mathbf{u}} - \overrightarrow{\mathbf{u}_{p}}) + \frac{\overrightarrow{g}(\rho_{p} - \rho)}{\rho_{p}}$$
(1)

The left hand side of this equation, expresses the inertial force per unit mass, in which $\overrightarrow{u_p}$ is the particle velocity vector (m/s). The first term on the right hand side is the drag force term and the second term is the gravity and the buoyancy terms, in which ρ and ρ_P are the density of air and particles (kg/m³), respectively. F_D is the inverse of relaxation time (s¹), computed by:

$$F_{D} = \frac{18\mu}{\rho_{p}d_{p}^{2}} \frac{C_{D}Re}{24}$$
 (2)

where μ is the fluid viscosity (kg/ms) and d_p is the particle diameter (m). Re is the Reynolds number based on relative velocity for each cartesian direction that is defined as

$$Re \equiv \frac{\rho dp \left| u_{p_i} - u_i \right|}{\mu} \tag{3}$$

The drag coefficient, CD, for smooth spherical particles is evaluated

using the expression provided by Morsi and Alexander (1972). That is

$$C_D = a_1 + \frac{a_2}{Re} + \frac{a_3}{Re^2} \tag{4}$$

where a₁, a₂, and a₃ are constants.

The air velocity \overrightarrow{u} consists of the time averaged part \overrightarrow{u} that is computed by solving the RANS equations with the standard k- ε model and the instantaneous fluctuation velocity \overrightarrow{u} that needs to estimated. Typically, u_i' is modeled using the discrete random walk (DRW) model. Accordingly,

$$u'_{i} = \xi \sqrt{\overline{u'_{i}^{2}}} = \xi i \sqrt{\frac{2k}{3}}$$
 (5)

where k is the turbulence kinetic energy and ξ_i is a Gaussian random number. The random value is kept constant over an interval of time given by the characteristic lifetime of the eddies. $\overrightarrow{u} = \overline{u_i} + u_i'$ is replaced in the particle momentum equation. Because of the assumed particle size of 2 μ m the Brownian diffusion effect is negligible (Zhang and Chen (2007)).

Using the described method, the airflow and the Lagrangian particle trajectories are evaluated. On the other hand, it is more common to describe the dispersion of particles or pollutant in environments such as in subway stations in term of concentration distribution. The Lagrangian method, however, does not directly provide for the particle concentration. The particle concentration is calculated by the following equation:

$$C_{j} = \frac{\dot{M} \sum_{i=1}^{m} dt(i,j)}{V_{i}}$$
 (6)

where \dot{M} is the number flow rate of each trajectory (kg/s), C_j is the mean particle concentration in the jth cell (kg/m³), V_j is the volume of the jth computational cell (m³), and subscript (i,j) represents the ith trajectory and the jth cell, respectively. The particle concentration in a cell can be calculated by counting the number of trajectories passing through the cell at the end of each time step. Zhang and Chen (Zhang and Chen (2006); Zhang and Chen (2007)) among other used this method.

When particles reach main doors or air conditioning units, they will escape and their trajectories are terminated. The trap boundary condition was used for the interaction between particles and all walls of the domain. Possibility of refection of the particles from the walls in complex geometry of the metro system is a complex phenomenon and depends to many parameters. Hence, as a first step to 3D simulation of the unsteady particles tracking in subway tunnels and stations, two extreme conditions were considered that for the first case the rebound possibility of the particles from the walls was neglected and the trap boundary condition was used for the interaction between particles and all walls of the domain. For the second case however, the reflect boundary condition was also tested and explained in the appendix.

3.1.2. Particle characteristic

3.1.2.1. Particle size and material. As it was mentioned by different studies, in the coarse particle region, a peak of around 2 μm in diameter was observed for railway airborne wear particles (Shen and Gao (2019); Olofsson et al. (2009); Abbasi et al. (2012b)). It is good to note that the fine nano particles needs more consideration due to the impact of Brownian motion and may be studied in future works. But for particles in the coarse region, the same results can be obtained. Fig. 3a shows that the results of average particle concentration for particle size of 1, 2 and 6 μm are roughly the same in different defined surfaces inside the domain.

All of the previous researches express that most of particulate matter in subway contain Fe (Jung et al. (2010)). Therefore, spherical particles of 2 μ m in diameter are considered and the density of particles is assumed to be 7874 kg/m³, which is the density of the dominating iron elements.

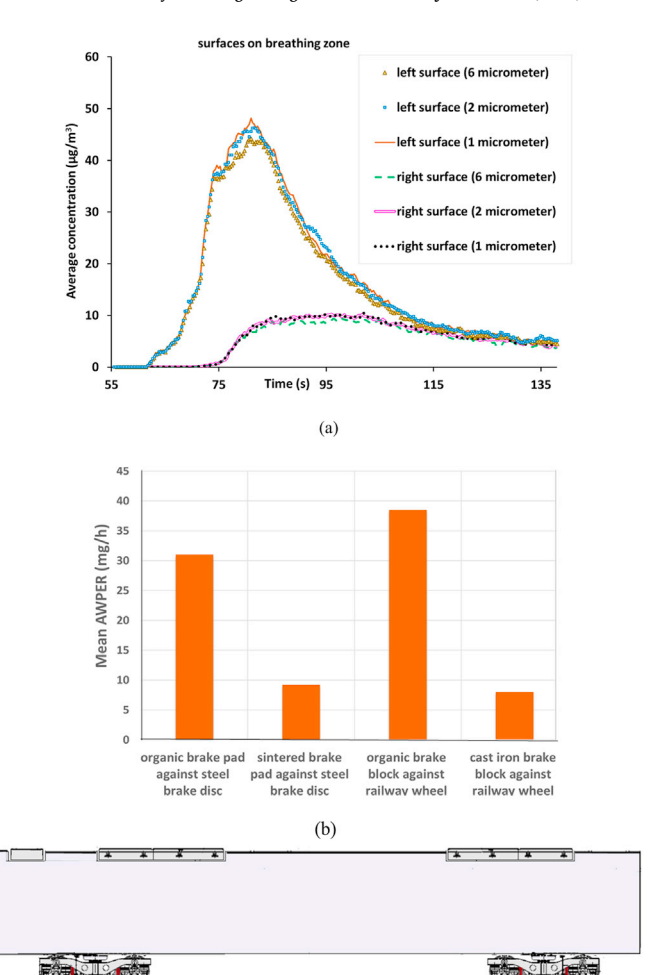


Fig. 3. (a) Comparison between average particle concentration for particle size of 1, 2 and 6 μ m, on planes located 1.5 m above the platform floor (b) Typical \overline{AWPER} values for different braking materials, measured by pin-on-disc set up of Abbasi et al. (2012a) (c) Schematic diagram of train car and its bogies with focusing on brake pads positions.

(c)

3.1.2.2. Particle emission rate. Abbasi et al. (2012a) presented an index for measuring and comparing wear particle emissions. The particles were generated from the wear of braking materials by a pin-on-disc tribometer equipped with particle measurement instruments. Generally, some of the wear particles become airborne during wear process. This can be characterized with the airborne wear particle emission rate (AWPER). AWPER is defined as the ratio of the generated airborne particles mass (in mg) to the time duration (in h) that two objects are sliding against each other under controlled conditions. Fig. 3b illustrates the results for mean wear airborne emission rate (AWPER) for different brake pad materials (Abbasi et al. (2012a)). For the results presented in this figure, the sliding velocity is 12.4 m/s, and the applied load is 60 N. This test condition is mostly representing the real subway train operational situation. For example, the 12.4 m/s sliding velocity represents the train braking at 70 km/h. The organic brake pad is considered for the present simulation. Therefore, the particle emission rate is assumed to be 32 mg/h. It should be noted that the contact surface was $8 \times 10^{-5} \text{m}^2$ in the pin on disc experimental set up of Abbasi et al. (2012a). The actual contact surface in brake pad is 0.026 m². Thus for the present numerical simulation, the emission rate was calculated to be 2.5 $\times\,10^{-6}$ kg/s for each of forty brake pads.

The number of injected particles is determined so that by increasing their number, the particle concentrations and depositions increase with the same proportion. Therefore, based on particle number study, around 3,600,000 particles are injected during braking in the time duration of t=55s to t=75s.

3.1.2.3. Particle injection position. The friction between brake pads and wheels is considered as a source of particle emission. As it was mentioned before, a subway train with five passenger cars was considered for this simulation. As shown in Fig. 3c each passenger car has eight wheels. Therefore, there are forty wheels and brake pads for each subway train. The surfaces of injecting particles can be assumed to be located around the brake pads positions. Therefore, particles are injected into the domain from these surfaces during the simulations.

3.2. Model validation

To verify the accuracy of the present numerical model, the results were compared with three sets of experimental data or empirical correlations available in the literature. The first one, which was used for validation of flow field, was the study of Kim and Kim (2007). They analyzed the train-induced unsteady flow in the tunnel, experimentally and their experimental results have been widely used by many researchers (Liu et al. (2018), Huang et al. (2010), Cross et al. (2015)). The comparison between the predictions of the present numerical model and their experimental data was presented in the recent previous work of the authors (Izadi et al. (2019)). Those who interested are referred to that article for more information about geometry, boundary conditions, flow validation and time-variations of the flow field inside the underground subway system. In addition, in other our recent work, another validation has been presented for the time variation of pressure inside the tunnel in comparison to some empirical correlations (Izadi et al. (2020)).

The other experimental data was used for validation of contaminant transport induced by a moving body. The available experimental data for dispersion of the micro-particles from a moving source is quite rare. Most of the particle distribution experimental data related to a moving boundary, are for the cases in which the particle source emission is fixed and the effect of moving body on particle distribution is investigated (Cao et al. (2017); Ren et al. (2019)), while in the present model, the particles are emitted from a moving boundary of train. Only Poussou et al. (2010) conducted 10:1 small-scale model experiments and investigated the effects of a moving human body on flow and contaminant transport inside an aircraft cabin. Experiments were performed in a water based model and the flow field and contaminant transport were measured. The aircraft cabin model was simplified to a half-cylinder, the human body was simplified to a cuboid and the cabin environmental control system

(ventilation with flow rate of 25 L/s) was considered. The body moved at the central line of the cabin model with a uniform speed of 0.175 m/s. The schematic diagram of their experimental set up is shown in Fig. 4. Some other researchers investigated the effect of moving particle source used their experimental data for their validation (Wu and Gao (2014)).

They simulated contaminant by injecting a dye into the flow and observing its fluorescence under laser illumination. The dye was released from the lateral sides of the moving body at flow rate of 25 mL/s (Fig. 4). They also used a CFD model with a combined dynamic and static mesh scheme of Fluent, and compared their computed average flow fields with the measured phase-averaged flow fields. Fig. 5 shows the comparison between the results of normalized concentration (C/C_{max}) obtained by present numerical model and the experimental and numerical results of Poussou et al. (2010). At t = 0, the distance between the cabin cross-section and the back of body is 9.4 cm. The fixed laser sheet is located 43.6 cm from the cabin cross section. Frames 2 and 4 were acquired when the back of the body moved, respectively, 3.42 cm and 8.25 cm past the laser sheet. Fig. 5 shows a qualitative comparison of contaminant dye transport across the cabin cross section. The maximum contaminant concentration occurs behind the top two corners of the moving body. Over time, the contaminant concentration in the location of fixed laser sheet decreases. As shown in this figure, the present numerical model predicted the dye intensity profile and location of maximum intensity reasonably well.

Fig. 6 compares the experimental data and CFD results of Poussou et al. (2010) (Fig. 6a and c) with the present numerical model (Fig. 6b and d) predictions of the longitudinal velocity vector field and contaminant concentration. The present model was able to capture the vortex structure above the moving body and the flow structures inclined at 45° behind the moving body. Fig. 6c and d compare the CFD results of Poussou et al. (2010) with the present numerical model for the normalized contaminant concentration (C/C_{max}), where good agreement is seen.

Fig. 7 shows a comparison of the decay of contaminant concentrations across the cabin cross section as the body moves through it. This figure shows that the present numerical model can well estimate the change in the strength of dye concentration obtained by the measured data of Poussou et al. (2010).

Figs. 5–7 suggest that the present numerical model, using dynamic mesh method, can predict the characteristics of the flow and contaminant transport around a moving object.

The validated computational method is then used to simulate the airflow field and the particle distribution in the full scale subway system with four stations and the connected tunnels. The results are described in the subsequent sections.

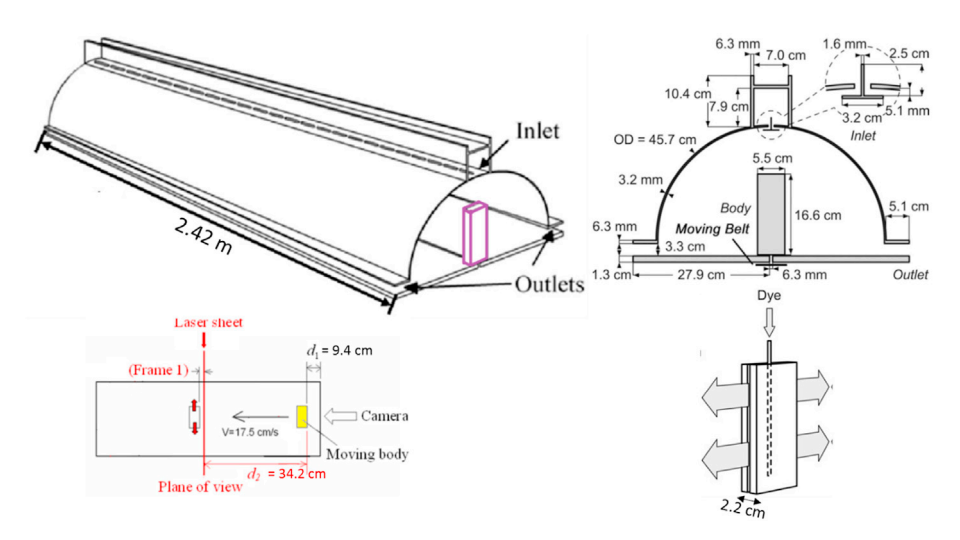


Fig. 4. Schematic diagram of experimental set up of Poussou et al. (2010).

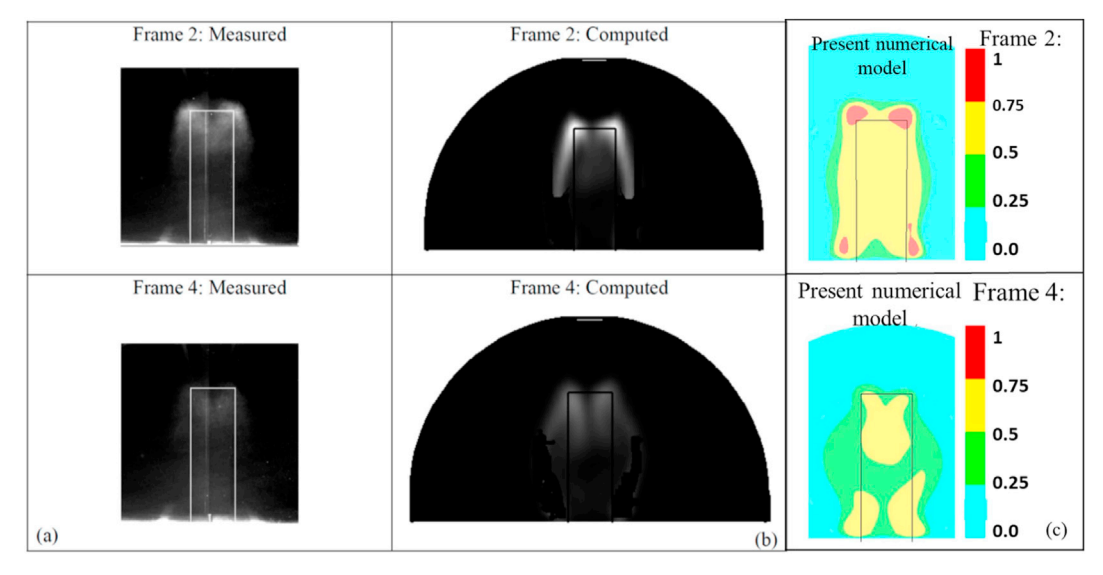


Fig. 5. Comparison between the results of normalized concentration in present numerical model and the experimental and numerical results of Poussou et al. (2010).

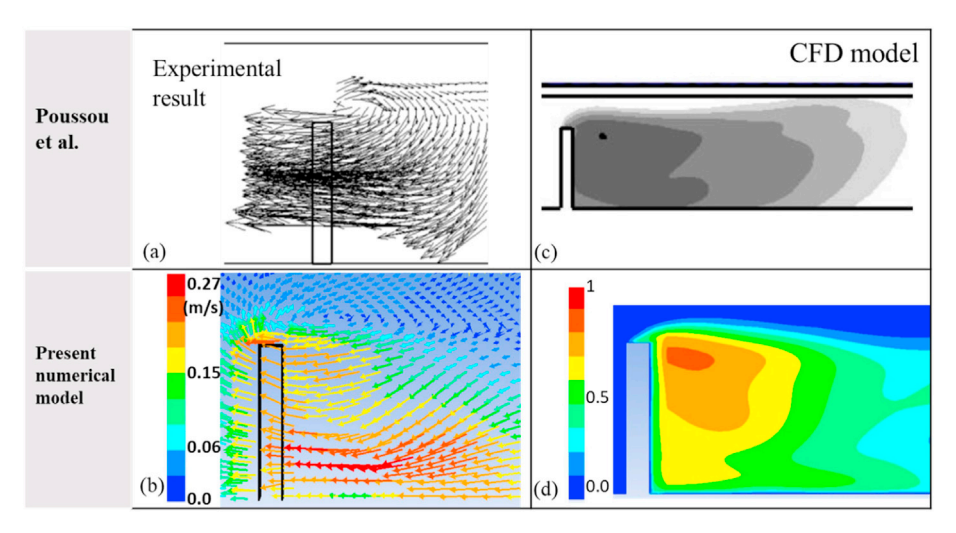


Fig. 6. (a) Mean velocity field measured by Poussou et al. (2010). (b) The present numerical model results for longitudinal flow field. (c) Results of CFD model by Poussou et al. (2010) for dye concentration. (d) The present numerical model results for dye concentration.

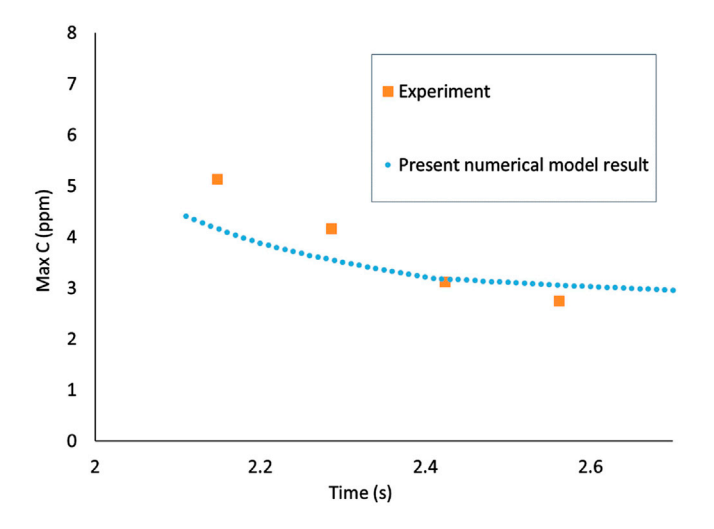


Fig. 7. Comparison of the present numerical model with the experimental data of Poussou et al. (2010) for the decay in maximum concentration.

4. Results and discussion

As it was shown in Fig. 1, the train is positioned in Station 2 at t = 0s. The exact profile of the train velocity depends to the length and slope of the tunnels, type of the electric motors and etc. In present work the train starts to move from Station 2 towards Station3 with a velocity profile which has been typically assumed in design of the ventilation system of a metro line (Kennedy (1976)) as shown in Fig. 8a. The train acceleration is 1 m/s² and its maximum velocity is 20 m/s which is the design maximum velocity for the metro train in Shiraz metro line. When the train approaches Station3 around t = 55s, it brakes with deceleration of -1 m/s^2 . As it was mentioned before, the particle generation due to the train braking and the friction between brake pads and train wheels is one of the major sources of subway station particles. Therefore, the dispersion and distribution of this type of particles are considered in this study. The iron particles of 2 µm in size are released from the brake pads positions located on the lateral sides of the train. The particles are released during train braking (from t = 55s to t = 75) with the total emission rate of 10^{-} kg/s. From t = 75s till t = 120s the train stops in the Station 3 for passenger exchange. The train starts to run again at t = 120s. To see the particles deposition and to track their trajectories inside the station, the

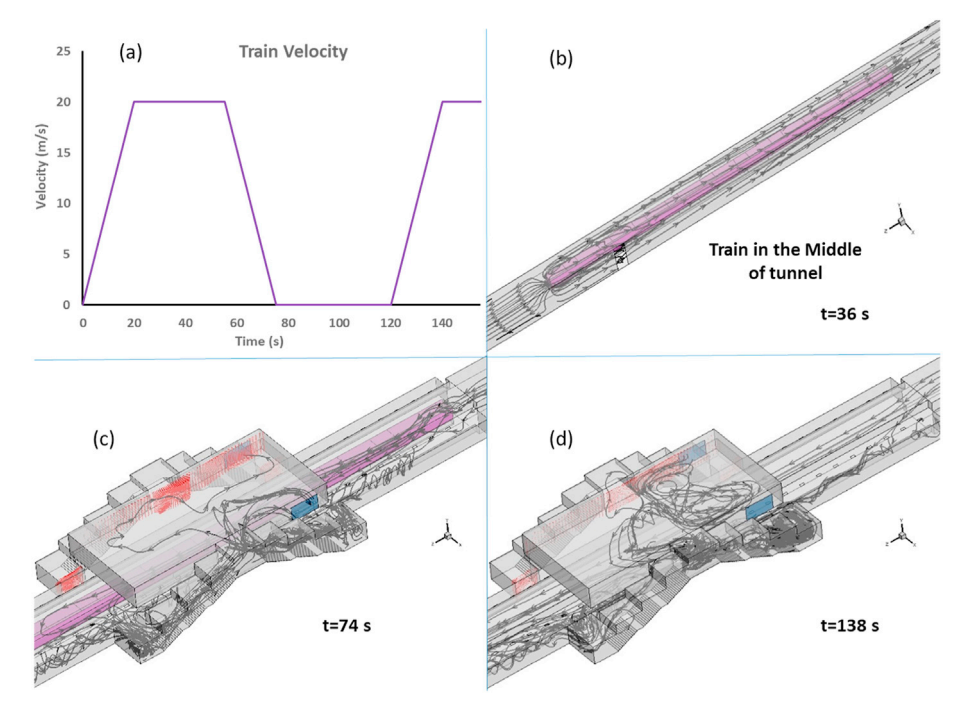


Fig. 8. (a) Speed of the train model (b) Streamlines around the train model; and time evolution of streamlines and airflow velocity vectors through way-outs with a focus on the right part of **Station 3** ((c) t = 74s (d) t = 138s).

computations are continued until t=150s, when the train is travelling inside the next tunnel.

4.1. Train induced flow field

For a moving train, the pressure in front of the vehicle increases while the pressure in the wake behind the train decreases. The forced airflow inside a tunnel caused by the moving vehicles is called the "piston effect". The streamlines around the train can be seen in Fig. 8b. The train head pushes the air like a piston and the main air stream in front of the train is created. However, a fraction of the airflow goes backward through the gap between the train and the tunnel. Because of the low pressure region around the train rear, the flow is pulled from Station 2 towards the train rear. Also the airflow coming from the train front spins back to the train rear and some of that makes a vortex. Therefore, more complex flow patterns are observed around the train rear.

Fig. 8c and d illustrate the streamlines of the airflow passing through the way-outs in Station3 at different times with a focus on the right part of the station. The train head and tail enters the tunnel, respectively, at t=61s and t=73s. When the train approaches and enters the station, it causes the air flow to enter and spread throughout the platform. Some parts of the injected air would flow to the ticket hall through the staircases. Airflow enters into the ticket hall and exits through the station main doors (Fig. 8c). After passenger exchange, the train moves again at t=120s and the train head and tail exit the station at t=122s and t=134s, respectively. When the train exits the station, the airflow inside the platform is pulled by the train rear. So the direction of the airflow would be towards the train rear which is in the next tunnel. As a result, the airflow direction in the staircases and ticket hall changes and some recirculation region are formed in these sites (Fig. 8d).

4.2. Particle distribution

4.2.1. Particles distribution inside platform

In this section we studied the effect of airflow, mainly due to the piston effect, on motions of particles released from the braking system of the train inside the tunnels and in the station. Fig. 9 illustrates the time

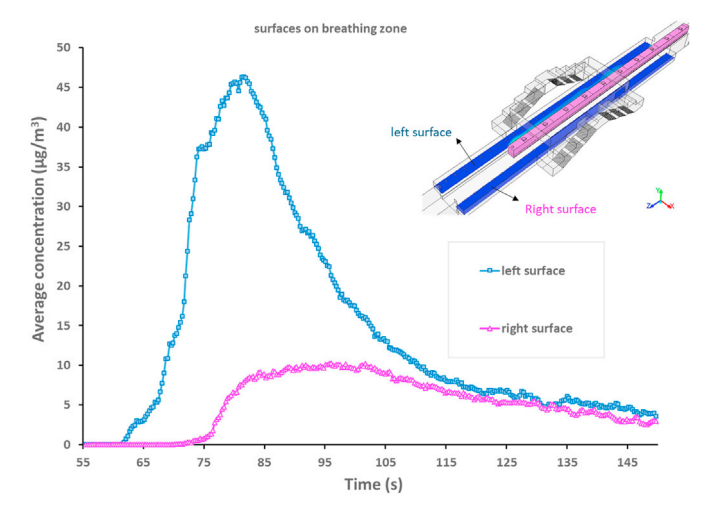


Fig. 9. Average particle concentration on the planes located 1.5 m above the platform floor, on the left and right platform.

variation of particle concentration in the human breathing zones on the left and right sides of platform. The surfaces are considered in the platform and 1.5 m above its floor. The left side plane is near the track side in which the train runs and the right side plane is near the other track.

As shown in Fig. 9, when the train enters the station (t=61s) the particle concentration in the left platform increases sharply up to 45 $\mu g/m^3$. The train stops in the station at t=75s. The particle concentration decreases with time after t=85s.

Fig. 9 also illustrates the time-variation of particle concentration on the right platform. Since the train model is travelling on the left track, it takes more time for the particles to reach this surface and for the concentration to increase. It is seen that the particle concentration on the right surface starts to increase at about t=68s. The maximum particle concentration reaches to only about $16~\mu\text{g/m}^3$, which is about a third of the particle concentration on the left track. The particle concentration on the right surface decreases slowly after t=100s. The particle

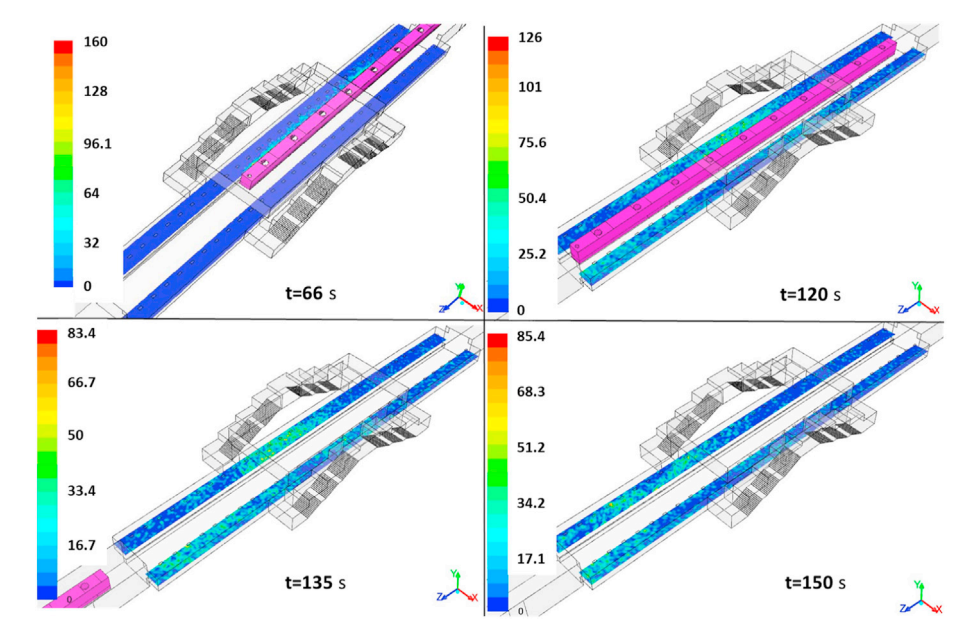


Fig. 10. Contours of particle concentration $(\mu g/m^3)$ on left and right surfaces at the breathing zone inside the platform at different times.

concentration on the left and right surfaces are become comparable after about t=120s.

Fig. 10 shows the contours of particle concentration on the planes at the human breathing zones on left and right sides of platform at different times. It is seen from this figure that the particle concentration on the surfaces varies with time. When the train is entering the station (t = 66s), the particle concentration increases particularly near the train vicinity. When the train is stopping at the station, the particles spread into the platform. At t = 120s, the maximum concentration on the left platform occurs between two way-outs while for the right platform, the peak concentration is near the station outlet. The train starts to move again at t = 120s. When the low pressure region of the train rear goes out of the station completely at about t = 134 s, it pulls the air and the suspended particles through the next tunnel. Thus, the maximum concentration occurs near the next tunnel inlet for both surfaces.

As noted before particles are generated when the train is braking. Because of the flow pattern around the train shown in Fig. 8b, most of the generated particles would be pushed to the train rear. These particles, however, move along with the train movement. Thus, the particles generated inside the tunnel flow toward the station. To study the amount

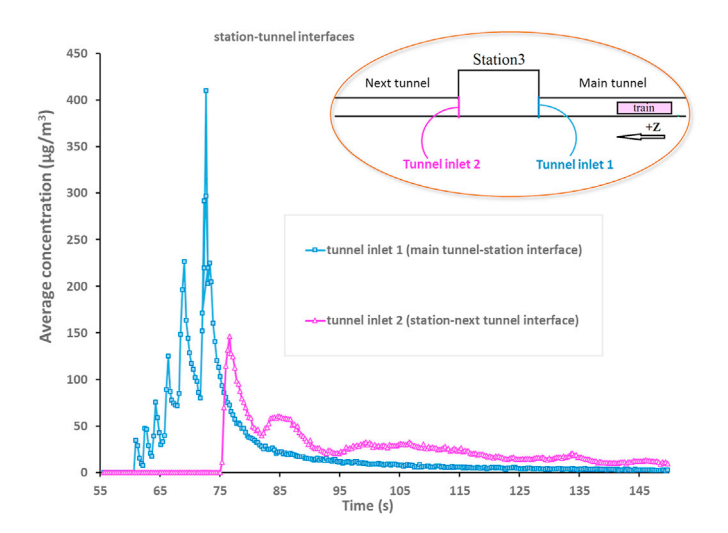


Fig. 11. Average particle concentration on the planes connecting the station to the tunnels (tunnel inlet 1 and tunnel inlet 2).

of particles coming from the tunnel into the platform, the particle concentration on the station entrance from the main tunnel (tunnel inlet 1) is shown in Fig. 11. As can be seen from this figure, when the train reaches the main tunnel-station interface at t=61s, the particle concentration on this plane starts to increase. The concentration reaches its peak, when the train rear leaves the plane at t=73s. Other fluctuations of concentration time history shown in Fig. 11 up to time t=73s, are related to the brake pads positions. When the brake pads positions pass the inlet plane, the particle concentration increases slightly and then it decreases again. After t=75s, the particle concentration decreases monotonically with time.

Fig. 11 also illustrates time-variations of the particle concentration on the station exit to the next tunnel (tunnel inlet 2). It is seen from this figure that the particle concentration on the exit plane (station-next tunnel interface) increases sharply at $t=75\mathrm{s}$. Although the train stops at the station at this time, some particles spread into the next tunnel. This is because of the continuation of piston effect. Since there are no particle generation after the train stops at the station and particles are trapped by the train and station walls, the particle concentration on exit plane decreases with time. It is also seen that the number of particles moving to the next tunnel increases slightly around $t=85\mathrm{s}$. This can be due to the particles generated from the nearest brake pad which were pushed towards the next tunnel as a result of the continuation of the piston effect. In addition, when the train rear, leaves the station completely at $t=134\mathrm{s}$, it pulls the air and particles out of the platform. Therefore, at this time the particle concentration at the exit plane increases slightly.

4.2.2. Particles passing through way-outs

As noted before, wear particles are mainly generated in the subway tunnels, disperse throughout the tunnels and platforms and spreads into the ticket hall and exhaust into the ambient air outside. As described earlier, there are four way-outs in the studied platform station. The names of way-outs are introduced in Figs. 1b and 12a. As shown in these figures, way-out openings are the surfaces that connect the platform to the staircases. The left side way-outs are on the track side in which the train runs and the right way-outs are on the other track. Considering the train movement along the +z direction, the first way-outs are named Way-out-1 (right and left) and the next set are named Way-out-2. The average particle concentration on each way-out represent the amount of particles that penetrates into the staircases and spreads to the ticket hall. Fig. 12b illustrates time-variation of average particle concentration on different way-outs.

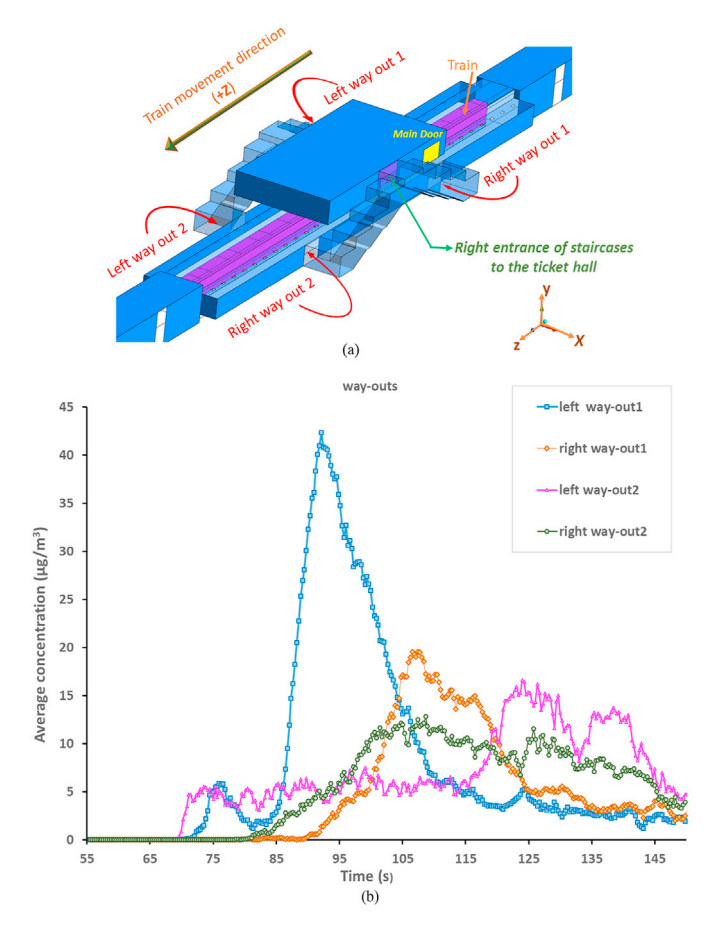


Fig. 12. (a) Schematic diagram of station model with platform way-out names (b) Time-variation of average particle concentration on different way-outs.

When the train enters the station while braking, it brings some wear particles that spreads in the platform. This causes the particle

concentration to start to increase at about t=75s. Most generated particles, however, are accumulated near the rear of the train, and after the train stops these particles disperse into the station due to the airflow generated by piston effect that still continue. Particles then spread to the platform and penetrate into the staircases through way-outs. This causes the sharp increase in the particle concentration at the left Way out 1 at t=85s (Fig. 12b). The particles get to the left side way-outs sooner because the train is travelling on the left track. As was noted before, the particles are accumulated behind the train, hence the concentration reaches to the higher values at the way outs number 1 which are located close the train rear.

In addition, when the train stops until it starts to move at t=120s the airflow exits from all way-outs so that the particles also flow towards the staircases and ticket hall through way-outs. At t=120s the train starts to leave the station and at t=125s for way-outs number 1 and t=134s for way-outs number 2, the airflow direction changes and air enters the platform. This is because of the piston effect and the low pressure region behind the train. Therefore, after t=134s almost no particles are transported to the staircases and in fact some particles would flow back to the platform.

According to the coordinates defined in Fig. 12a, the x-direction is normal to the way-out planes. Fig. 13a and Fig. 13b show particles xvelocity component through left way-outs. According to the +x direction, the negative values of particle x-velocity component indicate that the particles are moving out of the platform towards the staircase. The positive value shows that the particles are flowing back towards the platform. As shown in Fig. 13a for the left way-out 1, the particle starts to get out of the platform at t = 75s. Most particles reach and pass through this way-out around t = 95s. The particle x-velocity component changes sign at about t = 125s, which means that particles flow back into the platform. For the left Way-out 2 (Fig. 13b), most of the particles arrive at the wayout at around t = 110s, because this way-out is farther away from the tunnel inlet. At around t = 134s, the particles change their direction and flow back into the platform through the left Way-out 2. In addition, it is seen from this figure that after t = 120s, the amount of particles passing through Way-out 2 is more than that from Way-out 1, especially, near the end of the simulation time at t = 150s. This trend is consistent with the results shown in Fig. 12b.

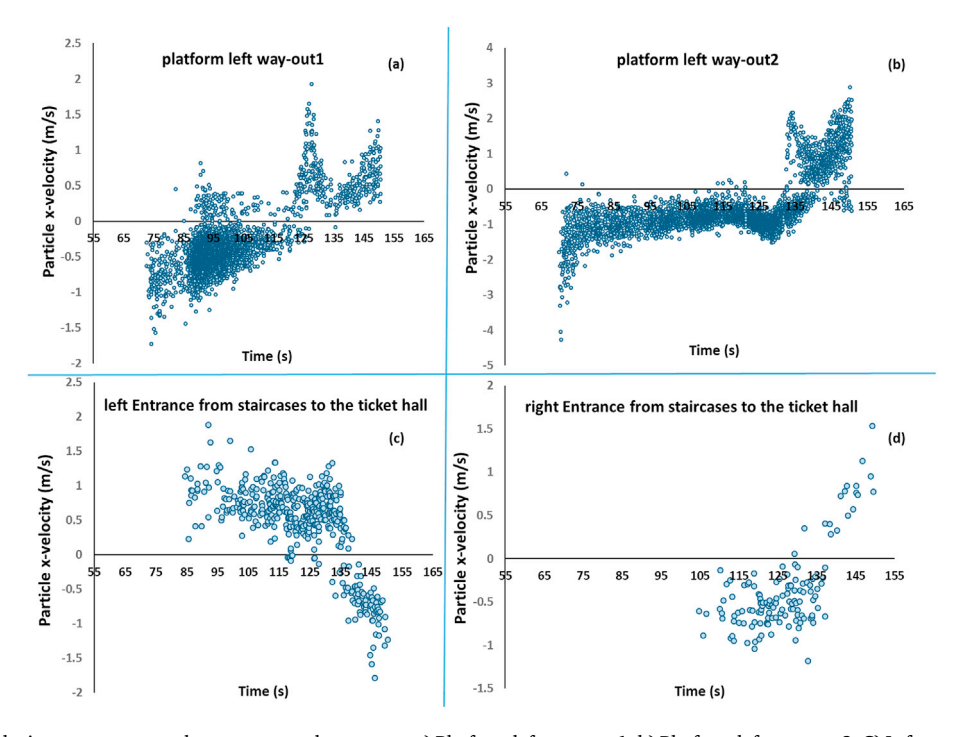


Fig. 13. The particle x-velocity component on the way-outs and entrances. a) Platform left way-out 1. b) Platform left way-out 2. C) Left entrance from staircases to the ticket hall. d) Right entrance from staircases to the ticket hall.

Figs. 13c and d show that some particles enter the ticket hall from the staircases. The particles start to enter the ticket hall from its left and right entrances, respectively, at $t=85 \, \mathrm{s}$ and $t=105 \mathrm{s}$. The entrances from staircases to the ticket hall are shown in Fig. 12a. It is also seen that more particles enter the ticket hall from left entrance. Some of these particles even leave through the left main door into the outside ambient air. It is good to mention again that when the train rear exits the station at $t=134 \mathrm{s}$, the particles change their direction and flow back into the staircases as are seen from Fig. 13c and d.

Fig. 14 illustrates the particle distributions inside the station at different time due to the piston effect. As was explained before, these wear particles are generated from the train braking. Because of the patterns of the streamlines around the train, no particles flow to the station before the train enters the station. When the decelerating train enters the station, it brings the particles that spread in the platform. Most of the generated particles are accumulated near the train rear (Fig. 14a). Thus, after the train stops, these particles enter the station with the airflow from tunnel and disperse around due to the continuation of piston effect. The Particles are distributed inside the platform and, in part, flow to the ticket hall through staircases (Fig. 14b). When the train completely exits the station at t = 134s, it causes the particles to be dragged to the station outlet so more particles are accumulated near the inlet of the next tunnel (Fig. 14c). Although the particles are partly trapped by the walls, a fraction of particles remain suspended in the tunnels, the platform and the ticket hall even at t = 150s (Fig. 14d). A video was prepared from the numerical results showing the motion of particles to provide a better understanding of the dispersion of particles inside the station. This video is available online in the supplementary materials for the readers. The video starts from the time that the train enters into the platform and shows the time evolution of particle distribution in the platform, staircases and ticket hall when the train stops for passenger exchange. The video continues until almost 5 s after the train departed from the station.

Supplementary video related to this article can be found at https://doi.org/10.1016/j.jweia.2021.104533

It should be emphasized that the results of the present study are in qualitative agreement with the experimental data of Moreno et al. (2014). They sampled at different positions along the platform and found that there are considerable lateral variations in PM concentrations along subway platforms, with the greatest accumulation of particulates usually occurring at one end of the platform. In addition, they showed that the position of passenger accesses (way-outs) markedly affect the PM concentrations. Those positioned at the train entry point induce more effective dilution (during train arrival) than those near the train exit point.

Salma et al. (2007) collected aerosol samples on the platform of a metropolitan underground railway station in downtown Budapest. They obtained their mass concentration data for a selected time interval during which a single train arrives, stops and departs at the station. They showed that the concentration increases when the train arrives. The peak in mass concentration occurred during the train arrival and was caused by the train as it entered the station. Then the concentration decays. The train departure pulled in some polluted air and therefore the mass concentration further decreased. Similar results are obtained in the present study for the time variation of particle concentration inside the platform, although the station geometry is not the same.

4.2.3. Particles entered the air conditioning system of the train

Martins et al. (2015a) reported that during a subway commuting travel, roughly 80% of the inhaled mass of subway $PM_{2.5}$ was deposited in the HRT (human respiratory tract). Despite the lower $PM_{2.5}$ concentrations inside the trains with respect to those on the station platforms, the highest dose was observed inside the trains due to longer exposure time. Therefore, it is important to evaluate the amount of particles that penetrate inside the train. In addition to the train doors, which open for passenger exchange, the only way for particles to enter the train, is through the train air conditioning systems, which are installed on the

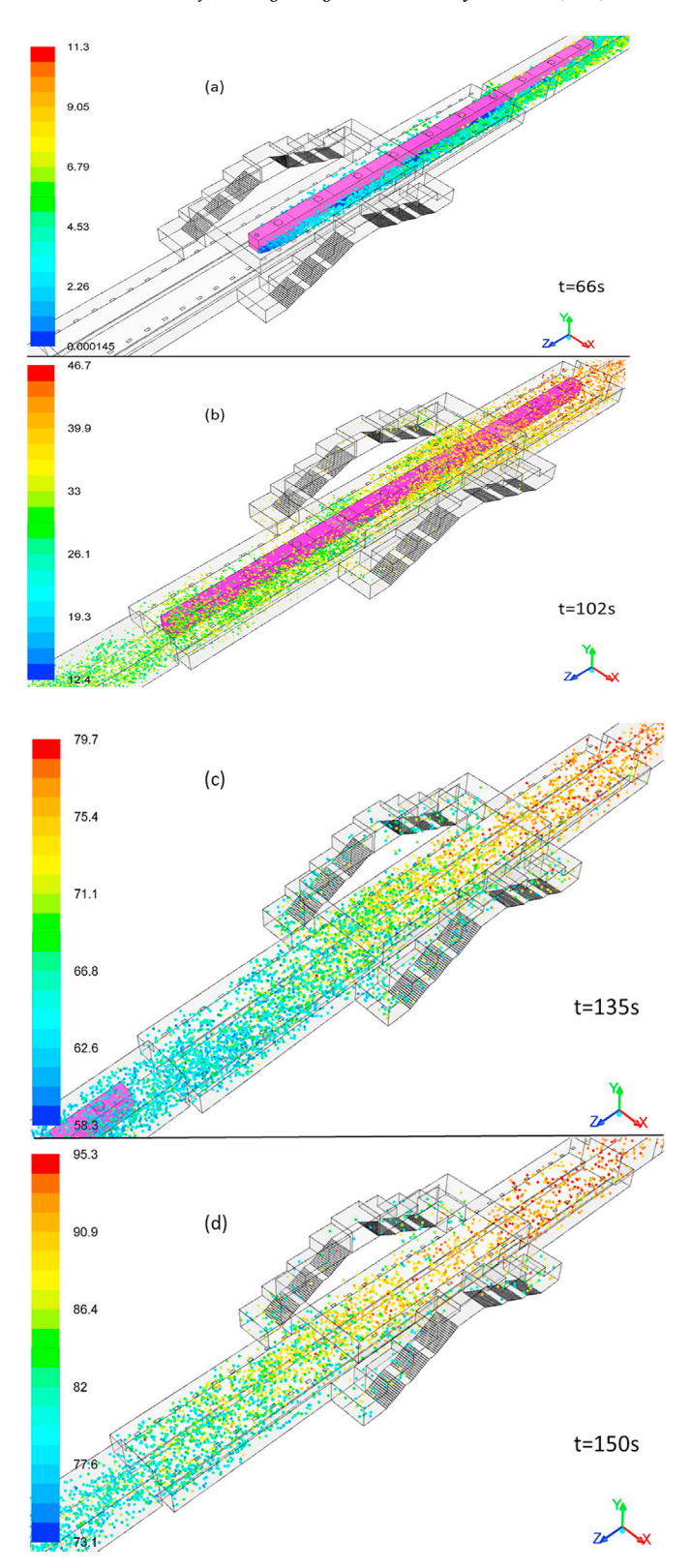


Fig. 14. Particles distribution inside Station 3 at (a) t = 68.2s, (b) t = 102s, (c) t = 135s, (d) t = 150s. The colors show the particle residence time. (For interpretation of the references to color in this figure legend, the reader is referred to the Web version of this article.)

train roof top. Fig. 15a shows a schematic diagram of a train body and the air conditioners on the train roof. Typically, the train has ten air conditioning units, which are installed in pairs in each of the five metro

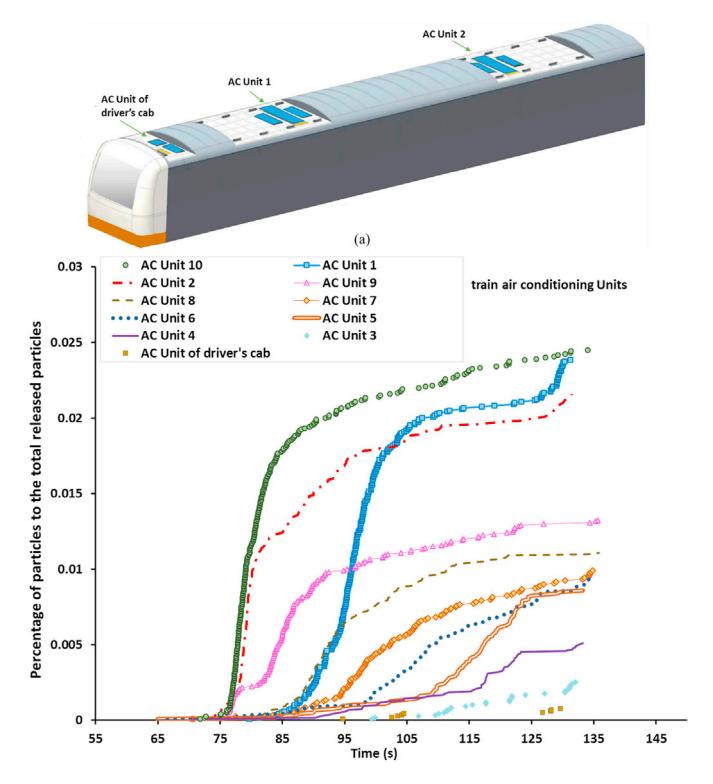


Fig. 15. (a) Schematic diagram of the train body (first passenger car) and air conditioner installed on the car roof (b) Percentage of particles passing through different air conditioning units on the train model.

wagons. The first wagon has an extra air conditioning unit for the driver's cab shown in Fig. 15. The structural pattern of the air conditioning unit is roof unit-type. Each unit is equipped with two sets of independent cooling systems with fresh air inlets at both sides of the unit. The fresh air enters the unit and is mixed with the return air in the compartments, and then fed into the air duct of the compartments after cooling (warming) treatment. Each air conditioning units has a ventilation rate of approximately 4000 m³/h (fresh air ≥ 1350 m³/h), while the air conditioning unit of the driver's cab has different characteristics with ventilation rate of approximately 800 m³/h (fresh air ≥ 60 m³/h). The flow rate at the air conditioning units, required in modeling the train, is defined by the aforementioned amounts of fresh air. The number of particles that penetrates inside the train through air conditioning units is shown in Fig. 15b.

Fig. 15b shows that the smallest number of entering particles corresponds to the driver's cab, and the maximum number of particles enters the train model through the last air conditioning unit (AC Unit 10). This result is expected because the driver's cab has the minimum amount of air ventilation rate. On the other hand, most of the particles were accumulated near the train rear and the number of entering particles is reduced from the train rear towards the train head. The only exceptions are the air conditioning units number 1 and 2 in which the number of entering particles is much higher compared to the others. This is due to the airflow variations in the platform and the streamlines around the train. In particular, Fig. 16 shows that a recirculation zone forms on top of the train body. This recirculation zone is created due to the piston effect and its interaction with the air that is flowing out through the way-outs 2. It is also seen that the recirculation zone is on the top of air conditioning units number 1 and 2. Therefore, the number of particles entering through these units increases.

Also, another result can be inferred from Fig. 15b. The particle generation and distribution starts at about t=55s but the particles enter the air conditioning units of the train model in the time interval of $75s \le t \le 135s$. So, it is concluded that, most of the particles enter

the air conditioning units during the train stop for the passenger exchange. In other words, when the train is running, the particle cannot enter the air conditioning systems; this is because of the high inertia of particles that are moving with fast airflow around the train. Therefore, one option for reducing the particle contamination is to partially or fully close the fresh air inlet of the air conditioning units during the train stop.

4.2.4. Particle deposition/suspension

Fig. 17 shows the amount of particles deposited on different surfaces in the time duration of 0 to t=150s. It is seen that about 58% of generated particles are deposited on the train body, 15% of particles are deposited in the main tunnel, while about 5% of generated particles remain suspended in the domain. Also 10% of particles conducted from the main tunnel to the station and 5% of particles moved from the station to the next tunnel, half of which are deposited in the next tunnel walls. Other particles are deposited in different surfaces of the station as illustrated in Fig. 17.

As noted before, a fraction of the particles flow from the platform into the ticket hall and even leave to the ambient air outside. Here about 0.05% of generated particles move into the ticket hall. Although the amount of these particles is small, the regular operation of the trains inside subway system can lead to a substantial amount of particles. It should be emphasized that the present simulation only takes into account the operation and braking of one train. While a large number of trains travelling daily in the metro system, which causes the accumulation and distribution of large amounts of particles.

It is worth noting that the present study can be considered as one of the first evolutions for numerical investigation of particle distribution due to train braking inside subway system, while more rigorous treatment may be required for an improved approximation to the exact physical phenomena. For example, in future studies train and brake pad accurate shape, different regimes of particle sizes and particle shapes can be considered, which one of the most important issue is the train shape especially the structures near the brake pad.

5. Conclusions

The dynamic mesh technique was used to simulate the 3-D flow around a moving train as well as the transport, dispersion and deposition of the train brake wear particles in an underground subway system. Firstly, an appropriate experimental data was used to estimate the amount of particle emission rate due to train braking. Also, the particle characteristics such as particle sizes or particle materials were determined. The numerical model of subway system consisting of 4 stations and connecting tunnels were simulated. It was validated by comparison with two sets of experimental data, which good agreements were observed. By using the validated model, the influence of piston effect on the spread of brake wear particles inside the station was analyzed. There are very few numerical studies considering the particle release and distribution from a moving source. The present work seems to be the first 3D numerical analyses about particle distribution due to train braking inside a complex domain of subway station.

When the train entered the station while braking, it generated and carried the brake wear particles into the platform. But because of the airflow around the train, most of the generated particles were accumulated at the rear of the train. After the train stops, these particles entered into the station due to the continuation of the piston effect. Particles then spread in the platform and penetrated into the staircases, ticket hall and even flowed to the outside ambient air.

Comparing the average particle concentration in the human breathing zones on the left and right sides of platform, it was found that the maximum concentration occurred on the left surface because the train was travelling in the left track. The particle concentration decayed after the train stops. When the train departed, the maximum concentration occurred near the next tunnel inlet for both sides.

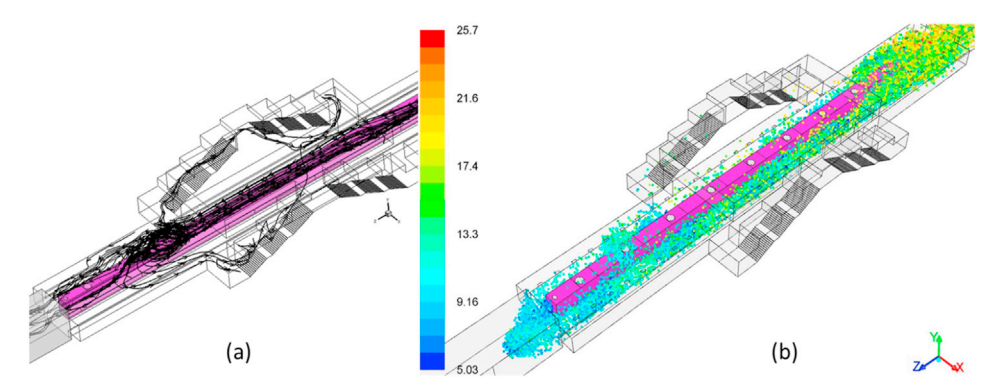


Fig. 16. (a) The streamlines pattern on top of the train body (b) Particle distribution around the train body at t = 81s (the color shows the particle residence time). (For interpretation of the references to color in this figure legend, the reader is referred to the Web version of this article.)

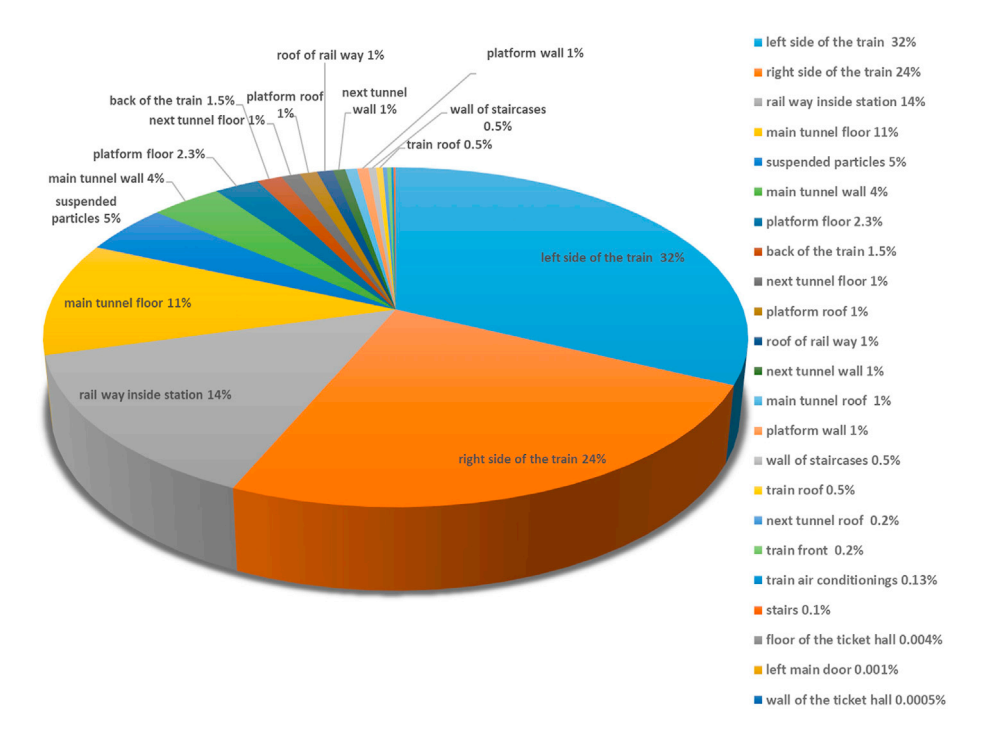


Fig. 17. The amount of particles deposited on different surfaces of subway system.

The particle emission rate of the train brake pad was calculated to be $2.5~\times10^{-6}$ kg/s. Subsequently, the average particle concentration due to train braking hits a peak of $45~\mu\text{g/m}^3$ and $16~\mu\text{g/m}^3$ for the left and right side of the platform, respectively. However, after train stop the concentrations decline and then level out at the amount of $5~\mu\text{g/m}^3$ for both right and left platforms. Almost 5% of generated particles due to train braking remain suspended in the domain and some of them move into the ticket hall. Therefore, the regular operation of the trains inside subway stations and tunnels can lead to a substantial amount of particles.

By simulating the airflow into the train air conditioning units, it was found that a fraction of particles would enter these units. The minimum and maximum numbers of entering particles were, respectively, for the driver's cab and the last air conditioning unit. The number of particles entering the train was reduced from the train rear towards the train head. The only exceptions were for the air conditioning units located under the recirculation zone, which was created near the train head.

CRediT authorship contribution statement

Tahereh Izadi: Methodology, Software, Formal analysis, Validation, Writing - original draft. **Mozaffar Ali Mehrabian:** Visualization, Supervision. **Goodarz Ahmadi:** Writing - review & editing. **Omid Abouali:** Conceptualization, Methodology, Supervision, Writing - review & editing.

Declaration of competing interest

All the authors declare that there is no potential conflict of interest including any financial, personal or other relationships with other people or organizations within that could in appropriately influence (bias) this work.

Appendix

When particles reach the entrances of station or air conditioning units, they will escape from computational domain and their trajectories are terminated. When reaching a wall, particles may either deposit or rebound from the surface of the wall. Particles in a ventilated room are most likely to attach to the surface since they usually do not have enough energy to overcome adhesion forces (Hinds (2012)). Particle will bounce from the surface if its kinetic energy at impact is larger than the van der Waals force (adhesion force). If the impact energy is low, it will be captured (trapped) by the wall. It is common to terminate, or trap, a particle trajectory after hitting a rigid surface. This treatment was used in many CFD studies of the indoor environment (Zhang and Chen (2006)). Therefore, as it was mentioned in the main body of the paper, the trap boundary condition was used for the interaction between particles and all walls of the domain. However, A semi-empirical relationship was presented by Cheng and Yeh (1979) indicating the inception of particle bounce. Based on their relationship, the particles do not bounce, if this condition is satisfied: $V_i d_p \le 5 \times 10^{-6}$ m²/s.

For the train-induced flow inside subway system, the airflow velocity in certain regions could become too high so there might be an uncertainty for the particle boundary condition at the wall. Therefore, the reflect boundary condition is also used for specific walls, so that particles are reflected from the wall surfaces if the above criterion occurred. In this way most of the particles hit the train body from t=55s till t=75s are reflected. The results for reflect and trap boundary conditions are compared in Fig. A-1. This figure shows that the trend of particle concentration is roughly the same but when applying reflect/trap boundary condition, the amount of particle concentration becomes much more than that for trap boundary condition. This is mostly because the particles that are trapped by the train body and/or the particles that are trapped in the gap between the train and the platform will be reflected in the domain. If these particles were not trapped, they might move to the platform and increase the particle concentration. This emphasizes the importance of the particles which might be reflected or bounced from the train and side walls of the railway in the platforms and their strong effect on increasing the PM pollutant level in the platforms. For this cases an UPE (Under Platform Exhaust) system can be very beneficial as it can remove these particles and reduces the pollution in the platform.

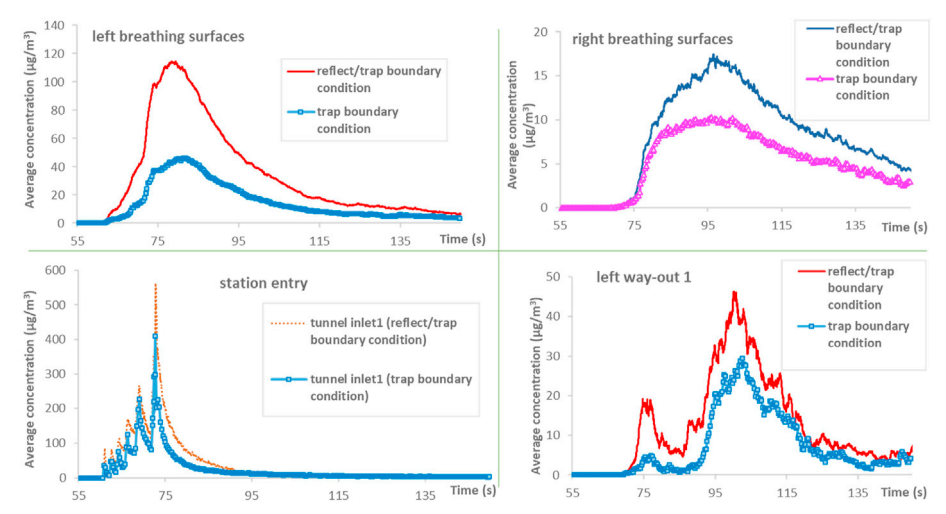


Fig. A-1. Comparison of the results of trap and reflect/trap boundary condition for wall surfaces in different regions of the domain.

References

- Aarnio, P., Yli-Tuomi, T., Kousa, A., Mäkelä, T., Hirsikko, A., Hämeri, K., Räisänen, M., Hillamo, R., Koskentalo, T., Jantunen, M., 2005. The concentrations and composition of and exposure to fine particles (PM2. 5) in the Helsinki subway system. Atmos. Environ. 39, 5059–5066.
- Abbasi, S., Jansson, A., Olander, L., Olofsson, U., Sellgren, U., 2012a. A pin-on-disc study of the rate of airborne wear particle emissions from railway braking materials. Wear 284, 18–29.
- Abbasi, S., Olander, L., Larsson, C., Olofsson, U., Jansson, A., Sellgren, U., 2012b. A field test study of airborne wear particles from a running regional train. Proc. Inst. Mech. Eng. - Part F J. Rail Rapid Transit 226. 95–109.
- Abbasi, S., Wahlström, J., Olander, L., Larsson, C., Olofsson, U., Sellgren, U., 2011.
 A study of airborne wear particles generated from organic railway brake pads and brake discs. Wear 273, 93–99.
- brake discs. Wear 273, 93–99.
 Birenzvige, A., Eversole, J., Seaver, M., Francesconi, S., Valdes, E., Kulaga, H., 2003.
 Aerosol characteristics in a subway environment. Aerosol Sci. Technol. 37, 210–220.
- Braniš, M., 2006. The contribution of ambient sources to particulate pollution in spaces and trains of the Prague underground transport system. Atmos. Environ. 40, 348–356.
- Cao, S.-J., Cen, D., Zhang, W., Feng, Z., 2017. Study on the impacts of human walking on indoor particles dispersion using momentum theory method. Build. Environ. 126, 195–206.
- Chan, L., Lau, W., Zou, S., Cao, Z., Lai, S., 2002. Exposure level of carbon monoxide and respirable suspended particulate in public transportation modes while commuting in urban area of Guangzhou, China. Atmos. Environ. 36, 5831–5840.
- Cheng, Y.-H., Lin, Y.-L., Liu, C.-C., 2008. Levels of PM10 and PM2. 5 in Taipei rapid transit system. Atmos. Environ. 42, 7242–7249.
- Cheng, Y.-S., Yeh, H.-C., 1979. Particle bounce in cascade impactors. Environ. Sci. Technol. 13, 1392–1396.

- Chillrud, S.N., Epstein, D., Ross, J.M., Sax, S.N., Pederson, D., Spengler, J.D., Kinney, P.L., 2004. Elevated airborne exposures of teenagers to manganese, chromium, and iron from steel dust and New York City's subway system. Environ. Sci. Technol. 38, 732–737.
- Colombi, C., Angius, S., Gianelle, V., Lazzarini, M., 2013. Particulate matter concentrations, physical characteristics and elemental composition in the Milan underground transport system. Atmos. Environ. 70, 166–178.
- Cross, D., Hughes, B., Ingham, D., Ma, L., 2015. A validated numerical investigation of the effects of high blockage ratio and train and tunnel length upon underground railway aerodynamics. J. Wind Eng. Ind. Aerod. 146, 195–206.
- Cui, G., Zhou, L., Dearing, J., 2016. Granulometric and magnetic properties of deposited particles in the Beijing subway and the implications for air quality management. Sci. Total Environ. 568, 1059–1068.
- Fridell, E., Björk, A., Ferm, M., Ekberg, A., 2011. On-board measurements of particulate matter emissions from a passenger train. Proc. Inst. Mech. Eng. - Part F J. Rail Rapid Transit 225, 99–106.
- Fridell, E., Ferm, M., Ekberg, A., 2010. Emissions of particulate matters from railways–Emission factors and condition monitoring. Transport. Res. D-Tr. E. 15, 240–245.
- Fromme, H., Oddoy, A., Piloty, M., Krause, M., Lahrz, T., 1998. Polycyclic aromatic hydrocarbons (PAH) and diesel engine emission (elemental carbon) inside a car and a subway train. Sci. Total Environ. 217, 165–173.
- Furuya, K., Kudo, Y., Okinaga, K., Yamuki, M., Takahashi, S., Araki, Y., Hisamatsu, Y., 2001. Seasonal variation and their characterization of suspended particulate matter in the air of subway stations. J. Trace Microprobe Tech. 19, 469–485.
- González, M.L., Vega, M.G., Oro, J.M.F., Marigorta, E.B., 2014. Numerical modeling of the piston effect in longitudinal ventilation systems for subway tunnels. Tunn. Undergr. Space Technol. 40, 22–37.
- Hinds, W.C., 2012. Aerosol Technology: Properties, Behavior, and Measurement of Airborne Particles. John Wiley & Sons.

- Huang, Y.-d., Wei, G., Chang-Nyung, K., 2010. A numerical study of the train-induced unsteady airflow in a subway tunnel with natural ventilation ducts using the dynamic layering method. J. Hydrodyn. B 22, 164–172.
- Izadi, T., Abouali, O., Mehrabian, M.A., Salmanzadeh, M., 2020. Investigation of the effects of different parameters on the generated pressure waves inside the tunnels. SN Applied Sciences 2, 1–13.
- Izadi, T., Mehrabian, M.A., Abouali, O., Ahmadi, G., 2019. 3-D numerical analysis of train-induced flow inside four ventilated underground subway stations and connecting tunnels. J. Wind Eng. Ind. Aerod. 193, 103974.
- Jiang, Z., Liu, T., Chen, X., Li, W., Guo, Z., Niu, J., 2019. Numerical prediction of the slipstream caused by the trains with different marshalling forms entering a tunnel. J. Wind Eng. Ind. Aerod. 189, 276–288.
- Johansson, C., Johansson, P.-Å., 2003. Particulate matter in the underground of Stockholm. Atmos. Environ. 37, 3–9.
- Jung, H.-J., Kim, B., Ryu, J., Maskey, S., Kim, J.-C., Sohn, J., Ro, C.-U., 2010. Source identification of particulate matter collected at underground subway stations in Seoul, Korea using quantitative single-particle analysis. Atmos. Environ. 44, 2287, 2293
- Kam, W., Cheung, K., Daher, N., Sioutas, C., 2011. Particulate matter (PM) concentrations in underground and ground-level rail systems of the Los Angeles Metro. Atmos. Environ. 45, 1506–1516.
- Karlsson, H.L., Nilsson, L., Möller, L., 2005. Subway particles are more genotoxic than street particles and induce oxidative stress in cultured human lung cells. Chem. Res. Toxicol. 18, 19–23.
- Kennedy, W., 1976. Subway Environmental Design Handbook. US Dep. of Transportation. Kim, J.-Y., Kim, K.-Y., 2009. Effects of vent shaft location on the ventilation performance in a subway tunnel. J. Wind Eng. Ind. Aerod. 97, 174–179.
- Kim, J., Kim, K., 2007. Experimental and numerical analyses of train-induced unsteady tunnel flow in subway. Tunn. Undergr. Space Technol. 22, 166–172.
- Kim, K.Y., Kim, Y.S., Roh, Y.M., Lee, C.M., Kim, C.N., 2008. Spatial distribution of particulate matter (PM10 and PM2. 5) in Seoul Metropolitan Subway stations. J. Hazard Mater. 154, 440–443.
- Knibbs, L.D., de Dear, R.J., 2010. Exposure to ultrafine particles and PM2. 5 in four Sydney transport modes. Atmos. Environ. 44, 3224–3227.
- Levy, J.I., Houseman, E.A., Ryan, L., Richardson, D., Spengler, J.D., 2000. Particle concentrations in urban microenvironments. Environ. Health Perspect. 108, 1051–1057.
- Li, Q., Loy-Benitez, J., Heo, S., Lee, S., Liu, H., Yoo, C., 2019a. Flexible real-time ventilation design in a subway station accommodating the various outdoor PM10 air quality from climate change variation. Build. Environ. 153, 77–90.
- Li, W., Liu, T., Huo, X., Chen, Z., Guo, Z., Li, L., 2019b. Influence of the enlarged portal length on pressure waves in railway tunnels with cross-section expansion. J. Wind Eng. Ind. Aerod. 190, 10–22.
- Liu, M., Zhu, C., Cui, T., Zhang, H., Zheng, W., You, S., 2018. An alternative algorithm of tunnel piston effect by replacing three-dimensional model with two-dimensional model. Build. Environ. 128, 55–67.
- Martins, V., Minguillón, M.C., Moreno, T., Querol, X., de Miguel, E., Capdevila, M., Centelles, S., Lazaridis, M., 2015a. Deposition of aerosol particles from a subway microenvironment in the human respiratory tract. J. Aerosol Sci. 90, 103–113.
- Martins, V., Moreno, T., Minguillón, M.C., Amato, F., de Miguel, E., Capdevila, M., Querol, X., 2015b. Exposure to airborne particulate matter in the subway system. Sci. Total Environ. 511, 711–722.
- Moreno, T., Pérez, N., Reche, C., Martins, V., de Miguel, E., Capdevila, M., Centelles, S., Minguillón, M., Amato, F., Alastuey, A., 2014. Subway platform air quality: assessing the influences of tunnel ventilation, train piston effect and station design. Atmos. Environ. 92, 461–468.
- Moreno, T., Reche, C., Minguillón, M.C., Capdevila, M., de Miguel, E., Querol, X., 2017. The effect of ventilation protocols on airborne particulate matter in subway systems. Sci. Total Environ. 584, 1317–1323.
- Morsi, S., Alexander, A., 1972. An investigation of particle trajectories in two-phase flow systems. J. Fluid Mech. 55, 193–208.
- Mugica-Álvarez, V., Figueroa-Lara, J., Romero-Romo, M., Sepúlveda-Sánchez, J., López-Moreno, T., 2012. Concentrations and properties of airborne particles in the Mexico City subway system. Atmos. Environ. 49, 284–293.

- Murruni, L., Solanes, V., Debray, M., Kreiner, A., Davidson, J., Davidson, M., Vázquez, M., Ozafrán, M., 2009. Concentrations and elemental composition of particulate matter in the Buenos Aires underground system. Atmos. Environ. 43, 4577–4583.
- Nieuwenhuijsen, M., Gomez-Perales, J., Colvile, R., 2007. Levels of particulate air pollution, its elemental composition, determinants and health effects in metro systems. Atmos. Environ. 41, 7995–8006.
- Niu, J.-q., Zhou, D., Liang, X.-f., Liu, S., Liu, T.-h., 2018. Numerical simulation of the Reynolds number effect on the aerodynamic pressure in tunnels. J. Wind Eng. Ind. Aerod. 173, 187–198.
- Olofsson, U., Olander, L., Jansson, A., 2009. Towards a model for the number of airborne particles generated from a sliding contact. Wear 267, 2252–2256.
- Poussou, S.B., Mazumdar, S., Plesniak, M.W., Sojka, P.E., Chen, Q., 2010. Flow and contaminant transport in an airliner cabin induced by a moving body: model experiments and CFD predictions. Atmos. Environ. 44, 2830–2839.
- Querol, X., Moreno, T., Karanasiou, A., Reche, C., Alastuey, A., Viana, M., Font, O., Gil, J., Miguel, E.d., Capdevila, M., 2012. Variability of levels and composition of PM 10 and PM 2.5 in the Barcelona metro system. Atmos. Chem. Phys. 12, 5055–5076.
- Raut, J.-C., Chazette, P., Fortain, A., 2009. Link between aerosol optical, microphysical and chemical measurements in an underground railway station in Paris. Atmos. Environ. 43, 860–868.
- Ren, C., Feng, Z., Cen, D., Cao, S.-J., 2019. Study on the subway environment induced by moving train using Gaussian distributed momentum source theory method. Indoor Built Environ. 28, 1083–1091.
- Ripanucci, G., Grana, M., Vicentini, L., Magrini, A., Bergamaschi, A., 2006. Dust in the underground railway tunnels of an Italian town. J. Occup. Environ. Hyg. 3, 16–25.
- Salma, I., Pósfai, M., Kovács, K., Kuzmann, E., Homonnay, Z., Posta, J., 2009. Properties and sources of individual particles and some chemical species in the aerosol of a metropolitan underground railway station. Atmos. Environ. 43, 3460–3466.
- Salma, I., Weidinger, T., Maenhaut, W., 2007. Time-resolved mass concentration, composition and sources of aerosol particles in a metropolitan underground railway station. Atmos. Environ. 41, 8391–8405.
- Seaton, A., Cherrie, J., Dennekamp, M., Donaldson, K., Hurley, J., Tran, C., 2005. The London Underground: dust and hazards to health. Occup. Environ. Med. 62, 355–362
- Shen, J., Gao, Z., 2019. Commuter exposure to particulate matters in four common transportation modes in Nanjing. Build. Environ. 156, 156–170.
- Sitzmann, B., Kendall, M., Watt, J., Williams, I., 1999. Characterisation of airborne particles in London by computer-controlled scanning electron microscopy. Sci. Total Environ. 241. 63–73.
- Sundh, J., Olofsson, U., Olander, L., Jansson, A., 2009. Wear rate testing in relation to airborne particles generated in a wheel-rail contact. Lubric. Sci. 21, 135–150.
- Wahlström, J., Söderberg, A., Olander, L., Olofsson, U., 2009. A disc brake test stand for measurement of airborne wear particles. Lubric. Sci. 21, 241–252.
- Wilcox, D.C., 2006. Turbulence Modeling for CFD. DCW Industries. Inc, La Canada, CA. November.
- Wu, Y., Gao, N., 2014. The dynamics of the body motion induced wake flow and its effects on the contaminant dispersion. Build. Environ. 82. 63–74.
- Xue, P., You, S., Chao, J., Ye, T., 2014. Numerical investigation of unsteady airflow in subway influenced by piston effect based on dynamic mesh. Tunn. Undergr. Space Technol. 40, 174–181.
- Yang, W., Deng, E., Lei, M., Zhang, P., Yin, R., 2018. Flow structure and aerodynamic behavior evolution during train entering tunnel with entrance in crosswind. J. Wind Eng. Ind. Aerod. 175, 229–243.
- Ye, X., Lian, Z., Jiang, C., Zhou, Z., Chen, H., 2010. Investigation of indoor environmental quality in Shanghai metro stations, China. Environ. Monit. Assess. 167, 643–651.
- Zarnaghsh, A., Abouali, O., Emdad, H., Ahmadi, G., 2019. A numerical study of the traininduced unsteady airflow in a tunnel and its effects on the performance of jet fans. J. Wind Eng. Ind. Aerod. 187, 1–14.
- Zhang, H., Zhu, C., Liu, M., Zheng, W., You, S., Li, B., Xue, P., 2017. Mathematical modeling and sensitive analysis of the train-induced unsteady airflow in subway tunnel. J. Wind Eng. Ind. Aerod. 171, 67–78.
- Zhang, Z., Chen, Q., 2006. Experimental measurements and numerical simulations of particle transport and distribution in ventilated rooms. Atmos. Environ. 40, 3396–3408.
- Zhang, Z., Chen, Q., 2007. Comparison of the Eulerian and Lagrangian methods for predicting particle transport in enclosed spaces. Atmos. Environ. 41, 5236–5248.